Heliyon 10 (2024) e25379

Contents lists available at ScienceDirect

Heliyon

journal homepage: www.cell.com/heliyon

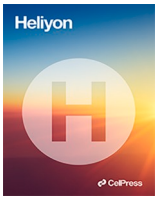

Research article

An Ogden hyperelastic 3D micromechanical model to depict Poynting effect in brain white matter

Mohit Agarwal, Assimina A. Pelegri *

Mechanical and Aerospace Engineering Rutgers, The State University of New Jersey, New Brunswick, NJ, USA

ARTICLE INFO

Keywords:
Micromechanics
Poynting effect
Numerical modeling
Axonal injury
Hyper-elastic materials
Mechanics of CNS white matter
Abaqus
Python

ABSTRACT

Shear and torsional load on soft solids such as brain white matter purportedly exhibits the Poynting Effect. It is a typical nonlinear phenomenon associated with soft materials whereby they tend to elongate (positive Poynting effect) or contract (negative Poynting effect) in a direction perpendicular to the shearing or twisting plane. In this research, a novel 3D micromechanical Finite Element Model (FEM) has been formulated to describe the Poynting effect in bi-phasic modeled brain white matter (BWM) representative volume element (RVE) with axons tracts embedded in surrounding extracellular matrix (ECM) for simulating brain matter's response to pure and simple shear. In the presented BWM 3D FEM, nonlinear Ogden hyper-elastic material model is deployed to interpret axons and ECM material phases. The modeled bi-phasic RVEs have axons tied to the surrounding ECM. In this proof-of-concept (POC) FEM, three simple shear loading configurations and a pure shear case were analyzed. Root mean square deviation (RMSD) was calculated for stress and deformation response plots to understand the effect of axon-ECM orientations and loading conditions on the degree of Poynting behavior. Variations in normal stresses (S11, S22, or S33) perpendicular to the shear plane underscored the significance of axonal fiber-matrix interactions. From the simulated ensemble of cases, a transitional dominance trend was noticed, as simple sheared axons showed pronounced Poynting behavior, but shear deformation build-up in the purely sheared brain model exhibited the highest Poynting behavior at higher strain % limits. At lower strain limits, simple shear imparted across and perpendicular to axonal tract directions emerged as the dominant Poynting effect configurations. At high strains, the stress-strain% plots manifested mild strain stiffening effects and bending stresses in purely sheared axons, substantiated the strong non-linearity in brain tissues' response.

1. Introduction

Mechanical response characterization and computational and mathematical modeling of brain tissues have gathered tremendous interest from researchers to comprehend the tissue's involvement in physiological and pathological conditions such as brain development, brain injury, and surgical procedures [1]. Brain tissues are one of the most intricate and compliant tissues in the human body. They are heterogeneous and exhibit highly non-linear elastic behavior. Because of their ultrasoft nature, they are sensitive to spatial and temporal resolutions. They exhibit hysteresis and highly non-linear response even when subjected to quasit-static loads or relatively small strains, making their characterization challenging [2,3]. Brain tissues also manifest loading-mode-specificity, as reported

* Corresponding author.
E-mail address: pelegri@rutgers.edu (A.A. Pelegri).

https://doi.org/10.1016/j.heliyon.2024.e25379
Received 20 September 2023; Received in revised form 11 January 2024; Accepted 25 January 2024
Available online 8 February 2024

by several research groups [2–5] who conducted a series of uniaxial or combined load tests to characterize brain matter. It is primarily attributed to the biphasic/heterogeneous nature of the brain tissues [3].

1.1. Characterization & modeling of brain tissues

Due to the above, acquiring consistent experimental data is challenging, therefore reliance on computational models for tissue characterization is of paramount importance. Regarding computational modeling of brain matter, parameter identification and choice of model non-linearity also play a crucial role in determining the degree of model congruence with experimental or actual biophysical phenomena. It was corroborated by findings from a viscoelastic parameter identification study from *Budday et al.* [6], in which they found that out of myriad loading scenarios, simple shear tests are apropos to describe the ultra-soft non-linear response of brain matter compared to pure tension or compression test setup. Their findings were in line with previous research from *Destrade et al.* [7] and *Rashid et al.* [8], who also observed that shear tests are promising compared to the other two modes since they are less susceptible to boundary effects and more resilient when subjected to large strains. This explains why there is a keen interest in the research community to develop time-dependent (dynamic strain rate) or time-independent (quasi-static) simple and pure shear experiments to identify and fit brain material parameters to known constitutive material physics. While shear testing protocols have received less focus from brain matter researchers than tensile or compression tests. Elaborate simple shear tests could help depict brain matter's incompressible isotropic and nonlinear elasticity. It could also aid visualize the underlying Poynting effect (Fig. 1(a)), a typical nonlinear phenomenon displayed by soft tissues such as brain white matter which is the primary phenomenon of focus in this proof-of-concept (POC) 3D FEM computational study.

Research has shown that mechanics are important in modulating brain function and dysfunctionalities [10]. Yet, an accurate assessment of mechanobiological processes in the brain necessitates advanced computational models that encapsulate the intricate and distinctive features inherent in the ultrasoft and profoundly non-linear heterogeneous brain matter. *Saccomandi et al.* [1] point out that most proposed constitutive models lack consensus despite all the efforts in modeling brain white matter (BWM). While much research has been invested into the mechanical characterization of brain matter, a huge variance in reported results and conflicting experimental observations have impeded progress in attaining reliable brain models. It is extremely challenging because of brain tissues' ultrasoft and heterogeneous nature, attributed to their distinctly nonlinear, rate-dependent, compression-tension asymmetric, and region-dependent behavior [4].

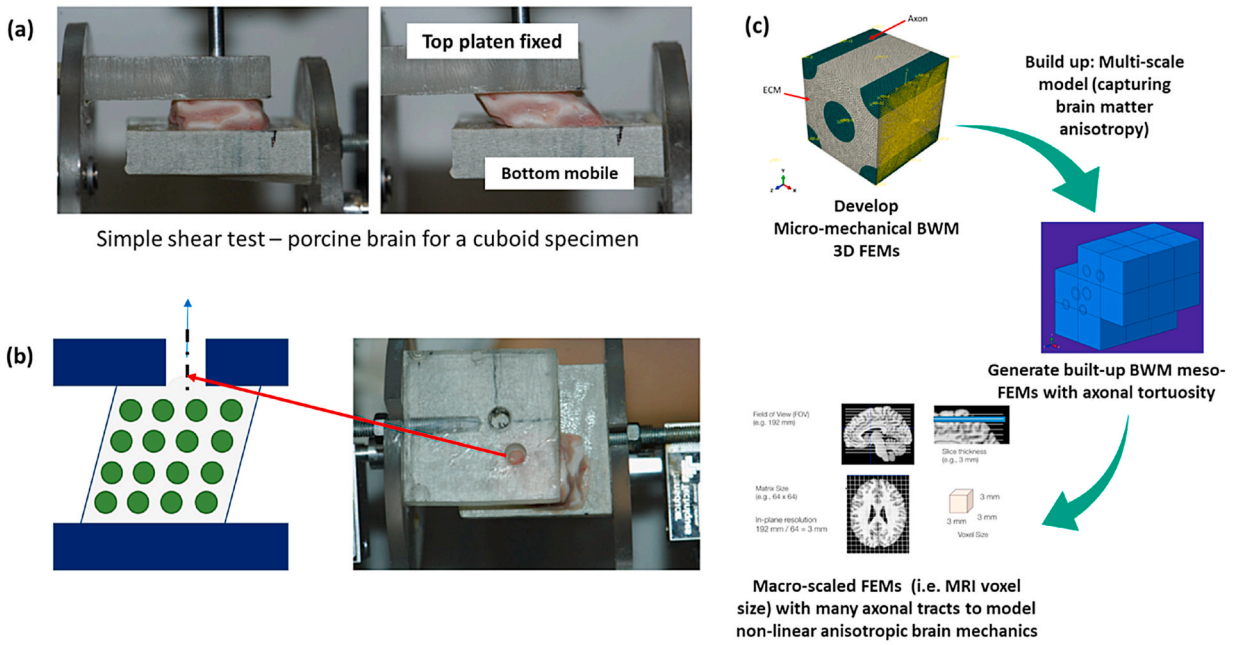

Fig. 1. (a) Simple shear testing of porcine brain matter. The top is fixed, and the bottom is mobile (adapted from Ref. [7]). (b) Schematics and experimental setup of the Poynting effect shown for the substantially large simple shear of porcine brain matter ($19 \times 19 \times 3$ mm). In the absence of platens, the sample expands in the 2-direction, as confirmed by drilling a hole in one platen and observing from the drilled platen that the exposed tissue area bulges out (adapted from Destrade et al. [7]). (c) Generate micro-mechanical FEMs to facilitate formulation of build-up (multi-scale) models incorporating brain white matter (BWM) axonal tract anisotropic properties to attain macro-scale high fidelity models (MRI voxels scale [9] RVEs) to simulate non-linear brain mechanics such as Poynting effect when subjected to shear.

1.2. Poynting effect and its practical implications

Another factor adding to the complexity of soft tissue characterization lies in experimental setups, which are often designed to use simple homogenous deformations in specimens, such as tension or compression, shear, torsion, or bi-directional homogenous deformations. Due to brain tissues' fragility and tackiness the use of dog bone-shaped test specimens to realize homogenous deformations over a substantial strain range is unattainable. *Destrade et al.* [7] researched different characterization methods to overcome these limitations. They identified simple shear and torsion tests at quasi-static rates as suitable candidates to obtain linear shear-stress and shear-strain relationships over a significant range of shear (up to 60%) [11,12]. Similarly, torque-angular displacement linear relationships were discovered by Shuck and Advani [13] and later confirmed by *Balbi* [14] and *Destrade* [15]. At the same time, compression tests can achieve homogenous deformation of only up to 10% strain, after which the specimen bulges out. In contrast, simple shear tests have worked well up to 45° tilt angles, attaining more than 60% stretch. Similar success has been reported with torsion tests of brain white matter.

The natural question arises as to why we are interested in simple shear and torsion tests. The reason is to examine the underlying *Poynting effect*, a typical nonlinear phenomenon exhibited by soft tissues such as brain white matter (Fig. 1(a and b)). When such materials are sheared or twisted, they dispose to either elongate (positive Poynting effect) or contract (negative Poynting effect [16] in a direction perpendicular to the shearing (rectangular specimen) or twisting plane (for cylindrical specimen) [17]. However, due to the lack of shearing devices capable of accurately quantifying and measuring these residual normal forces, further research is required to develop methodologies to help determine brain white matter properties. This is where the proposed research characterizes, and models brain white matter under shear loads.

Understanding the extent of the Poynting effect and characterizing its response to different shear-loading scenarios have many useful, practical implications. For instance, the Poynting effect influences reaction force and torque under extension-torsion loads applied biological materials. Researchers customarily examine the existence of Poynting effect in tissues using biomaterial analogs, such as polymers and hydrogels. As an example, the Poynting effect observed in soft hydrogels, courtesy of transient chemo-mechanical behavior and very large deformations, aids in designing and engineering functional polymers, which can then be used as sensors or actuators for heart tissue. These hydrogels manifest non-linear Poynting behavior, and proper characterization analytical modeling can aid in developing improved soft tissue control devises [18,19]. Case in point, tailored metamaterials can replicate natural tissue mechanics, facilitating a supportive environment for cell growth and tissue regeneration. *Ghorbani et al.* [20] proposed a novel study on the inverted and programmable Poynting effect in meta-materials. Their research identifies new avenues of programming the nonlinear elastic moduli in engineered materials and adjusting the couplings between shear and normal responses through rational design methodologies. Such inverted and programmable Poynting effects in metamaterials could inspire myriad applications, from designing enhanced contrast agents and implantable devices to engineering biological tissues operating under compression and torsion loads.

1.3. Research objectives of proposed Poynting 3D FEM

Since it is heterogeneous, brain biomechanics is largely influenced by the ultra-softness and non-linearity properties of white matter and fiber-matrix interactions. The microstructures and porosity in the brain tissues also determine the resultant degree of stiffness in brain tissues, as proven by experimental research outlined in previous sections. The proposed research aims to characterize the Poynting effect and determine its dependencies on material definition, load, fiber volume fraction, and geometry. This study confirms several key findings observed in similar experimental or analytical/numerical models in the past, such as the microstructural model from *Janmey et al.* [16] and *Rashid et al.* [8]. As summarized in **§3.5,** axon-matrix interaction did influence the magnitude of the resultant Poynting effect [21] compared to myriad shear load scenarios. From a practical standpoint in brain studies, this paper's findings suggest that the Poynting effect could be a vital physiological control mechanism [22], which could find many useful applications in surgical simulations or functional bio-polymer actuated sensor research and development. By adopting the Ogden hyper-elastic constitutive material modeling technique, comparative analyses (**§3.1 to §3.5**) of experimental slopes of resultant normal stress profiles proved that brain matter is extremely non-linear and resultant Poynting behavior is also non-linear when analyzed at quasi-static speeds. By proving the non-linear response of brain white matter to shear loads (observed positive Poynting effect), the current research also corroborated findings from *Destrade et al.* [7]. Our work supports Destrade's group claim that brain matter does not belong to the so-called "generalized neo-Hookean class," as Ogden model could effectively simulate non-linear shear response up to 100% simple and 60% pure shear in cubic bi-phasic modeled brain matter [7]. Directionality (positive or negative) and directional dominancy of the Poynting effect concerning shear load configurations have been major research topics. In this proposed POC 3D FEM, results indicated similar trends qualitatively in terms of robustness of Poynting effect, i.e. positive Poynting behavior was noticed for defined hyper-elastically modeled brain in all four evaluated shear configurations as elucidated in **§3** [23].

1.4. What is the significance of micro-mechanical FEM studies for the Poynting effect?

For this research, a micro-mechanical FE model has been formulated to analyze the Poynting effect in brain matter soft tissues when subjected to an ensemble of shear loads (simple and pure shear). As discussed previously, the characterization of brain matter is extremely challenging due to its inherent heterogeneity and high non-linearities. So, the choice of micro-scale FEM is to realize a long-term goal of attaining high-fidelity multi-scale computational models which could capture the anisotropic behavior of brain white matter (axons) from the micro and mesoscale FEMs/computational models and leverage these model outputs (stress and stiffness

response) for macroscopic voxels studies (i.e., *at scales of MRE/MRI imaging technologies*). A typical MRE/MRI voxel could encompass several axonal fiber tracts per voxel. Hence, an elaborate multi-scale hierarchical modeling approach would offer reliable and congruent analytics to surgeons and medical professionals in evaluating brain response custom to specific patients when subjected to traumatic brain injuries or other brain pathologies (acute or chronic) such as diffusional axonal injuries (DAI), impact or gradual aging-related tissue damage. As a succession study, scalable models with repeating blocks of micro-scale RVEs will be developed to realize this overarching goal (Fig. 1(c)). The proposed model would pave the way as a foundational study for depicting brain matter mechanics at the micro-scale, which are hard to characterize otherwise experimentally at the singular axonal level.

In this paper, a novel 3D micromechanical Finite Element Model (FEM) has been formulated in-house to simulate the Poynting effect in the bi-phasic Representative volume element (RVE). Previous research was utilized to determine the suitable volume fraction (VF) of axonal tracts embedded in the extracellular matrix (ECM) in white matter to model the bi-phasic RVEs for simulating the mechanical response under simple shear loads. Studies indicate that Ogden and Mooney-Rivlin models [8,24] have shown good agreement between experimental and numerical results to estimate normal forces (N) to depict the Poynting effect in soft solids. In this research, a nonlinear Ogden hyper-elastic constitutive material model has been deployed to characterize the bi-phasic RVE in 3D FEM. The brain's central nervous system (CNS) comprises white and gray matter. White matter comprises myelin-coated axons. Axons are long, slender projections of neurons that relay information to other neurons, muscles, and glands [25,26]. These axons are embedded in an extracellular matrix (ECM). In the proposed 3D FEM, axon-ECM comprises the bi-phasic constituents. For this proof-of-concept (POC) 3D RVE model, axon-ECM has been assumed to have pure affine boundary condition (i.e., the axon is tied down to the ECM) to capture axon-ECM interaction effects [27] on resultant Poynting behavior.

In total, three different simple shear cases: 1) shear along axon length, 2) shear perpendicular to axon fiber, and 3) shear across axon fibers were simulated to quantify the degree of Poynting behavior. A pure-shear RVE model was also analyzed to understand the role of fiber-matrix interactions on the brain's mechanical response to shear (Fig. 2(a–d)). Root mean square deviation (RMSD) was computed between normal stress-strain response plots for the ensemble in different simple shear configurations to depict axon-ECM orientations trends' role on dominant Poynting effect directions and resultant normal displacement (U). Variations in the degree of normal stresses (S11, S22, or S33) perpendicular to the shear plane in the analyzed three simple shear cases emphasized the role of fiber-matrix interactions and VFs (fiber dispersion) on PE [21]. At high strains, strain-stiffening effects were also evaluated from the stress-strain plots for the Ogden-modeled bi-phasic RVEs [11].

2. Materials and methods

2.1. Micromechanical finite element model

The microscale 3D FEM is developed in-house using Abaqus 2020 and Python scripting. Representative Volume Elements (RVEs) are formulated in single RVE units and compounded configurations to simulate simple shear in various configurations. In the current FEM, the average axonal diameter is modeled to be at 0.4395 μm (see Fig. 3(a and b)).

In the proposed 3D FEM, the axons and the ECM material characterizations are described by a non-linear Ogden hyper-elastic constitutive material model. The Ogden hyper-elastic model was motivated by its capability to accurately simulate large quasi-static strains (up to 100%) in very soft rubber-like materials.

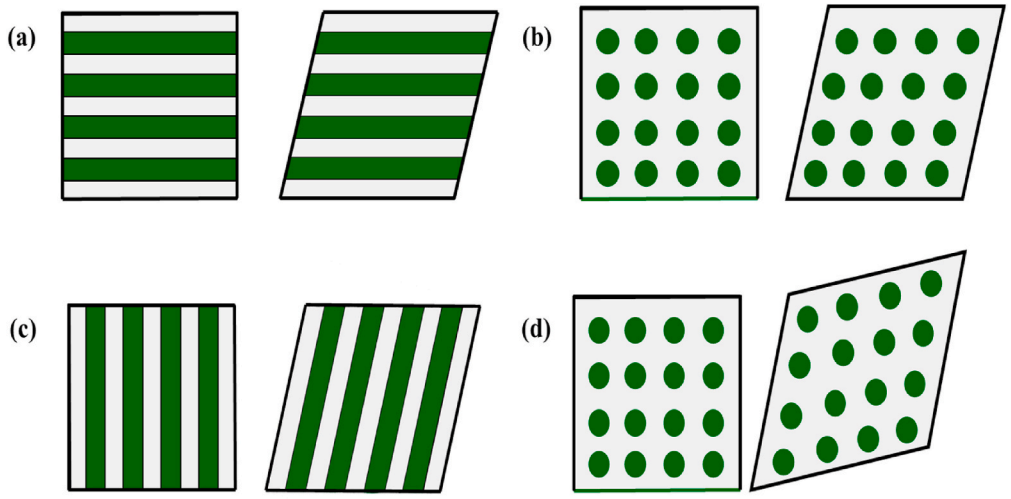

Fig. 2. Schematics of (a) longitudinal shear (along axon fiber axis), (b) shear across fiber (transverse shear), (c) shear perpendicular to axon fibers, and (d) pure shear strain case where shear strain is applied across both opposing axonal fiber faces. The dark green lines represent the axon fibers in (a) and (c), while the dark green circles depict the axon fiber cross-sections in (b) and (d).

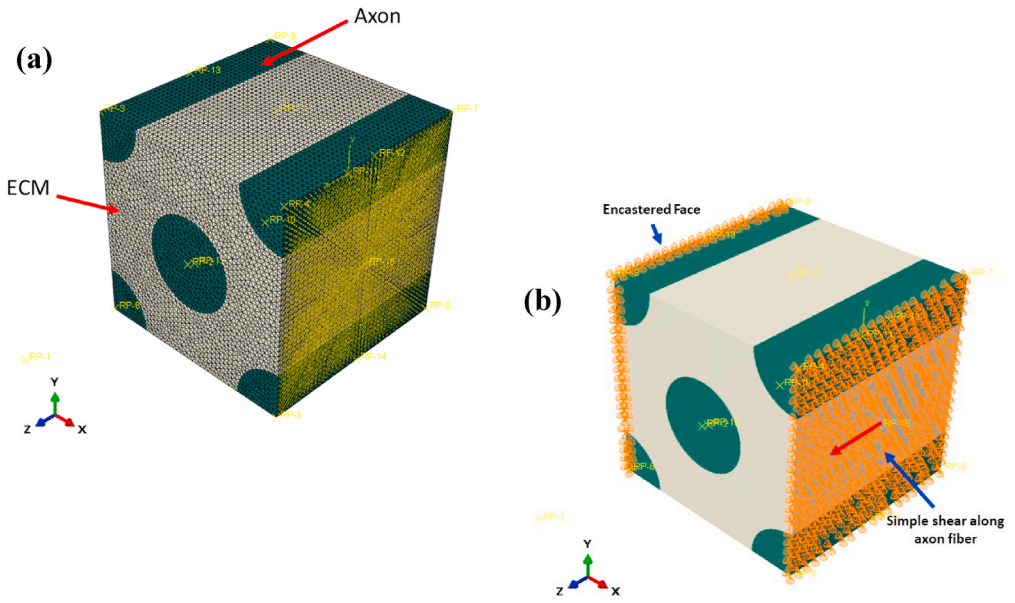

Fig. 3. (a) Single RVE FE Model of the ECM and axon bi-phasic assembly packing two axon fibers, volume fraction = 0.3. The ECM (light beige) and the axon fibers (dark green). (b) Boundary conditions for single RVE. The opposite surface is encountered (fixed) for simple shear, while the sheared face has the strain applied (along the axon fiber shown here). Contact between axons and ECM is defined to be fixed (tied) for this proof-of-concept (POC) FEM.

2.2. Hyper-elastic (HE) material model component

Nonlinear hyper-elastic materials models have been conventionally preferred for simulating soft biological tissues [28–32]. This research uses the Ogden hyper-elastic (HE) material model to depict the ECM and the axon phases [33]. This is because of their efficacy in accurately depicting nonlinear responses in neural tissue characterization at large deformations and strains by capturing the rate-dependent behavior (if modeled as Hyper-viscoelastic material) for dynamic strain rate scenarios. In the current study, the applied shear is quasi-static strain rates, and hence no rate-dependent behavior is applicable in this POC single RVE FEM study. The Ogden hyper-elastic model relies on three principal stretches, λ_1, λ_2, λ_3, and *2 N* material constants. This study specifically examines an incompressible, single-parameter Ogden hyperelastic material. The formulation of the strain energy density function, *W*, for the incompressible or nearly-incompressible Ogden constitutive (**Equation (1)**) in Abaqus is described as [33,34]:

$$W = \sum_{1}^{N} \frac{2\mu_i}{\alpha_i^2}\left(\overline{\lambda}_1^{\alpha_i} + \overline{\lambda}_2^{\alpha_i} + \overline{\lambda}_3^{\alpha_i} - 3\right) + \sum_{1}^{N} \frac{1}{D_i}(J_{el} - 1)^{2i} \tag{1}$$

where $\overline{\lambda_i} = J^{-\frac{1}{3}}\lambda_i$ and $\overline{\lambda_1\lambda_2\lambda_3} = 1$. Here, J denotes a local volume change and relates to the determinant of the deformation gradient tensor, via the right Cauchy-Green tensor $(C = F^T F)$ as $J^2 = det\,(F)^2$, μ_i Represents shear moduli. Meanwhile, α_i (stiffening parameter) and D_i are material parameters. In **Equation (1)**, J_{el} signifies elastic volume ratio. The first and the second terms signify the deviatoric and hydrostatic strain energy function components, respectively. The parameter $D_i = \frac{2}{K_0}$, allows for the inclusion of compressibility where K_0 is the initial bulk modulus. The same single parameter Ogden hyper-elastic material is also used in this research [35]. Therefore, N = 1. Incompressibility implies that $J_{el} = 1$ and is specified by setting $D_1 = 0$ in Abaqus. Abaqus removes the hydrostatic term, and the equation reduces to (**Eq. (2)**):

$$W = \sum_{1}^{N} \frac{2\mu_i}{\alpha_i^2}\left(\overline{\lambda}_1^{\alpha_i} + \overline{\lambda}_2^{\alpha_i} + \overline{\lambda}_3^{\alpha_i} - 3\right) \tag{2}$$

In the Ogden HE models, three principal Cauchy stress values are obtained by differentiating *W* with respect to λ. If an incompressible material is supposed to be subjected to uniaxial tension ($\sigma_y = \sigma_z = 0$). Then, the resultant hyper-elastic constitutive model principal stress $\sigma_{uniaxial}$, can then be expressed as **Equation (3)**:

$$\sigma_{uniaxial} = \frac{2\mu}{\alpha}\left[\lambda^{\alpha} - \left(\frac{1}{\sqrt{\lambda}}\right)^{\alpha}\right] \tag{3}$$

In this paper, as a POC FEM, axons are modeled as straight fibers and subjected to various shear modes. The constitutive equations describing resultant normal and shear stresses are explained in §2.3.

For the proposed FEM, the data for the axon and glia properties are taken from previous published work and literature [25,26,29,

30,36]. The values for shear modulus for the axons and ECM are derived from research by Wu et al. [37], α is obtained on the model proposed by Meaney [28]. The shear modulus of the ECM is specified relative to the axonal shear modulus, assuming that axons are three times stiffer than ECM, as described by Arborgast and Marguile's [38]. Model incompressibility for the HE material modeling component has been deployed the same as in Refs. [33,35]. Table 1 Summary of material properties μ, D and a, and element definition used in the simulation of single RVE- HE FEM.

2.3. Analytical modeling Poynting effect

Analytical modeling for describing the Poynting effect has been attempted using various constitutive models such as Neo-Hookean, Mooney-Rivlin, Blatz-Ko, St Venant-Kirchhoff, exponential, polynomial, Ogden, and some even utilized linear elastic material (generalized Hooke's Law) to describe Poynting effect [39]. This study will use the Ogden material model to derive constitutive relationships to analyze Poynting behavior in brain white matter. The formulations described only focus on highlighting key relationships, and the in-depth continuum mechanical model is out of the scope of this paper. Research from *Misra et al.* [39], *Rashid et al.* [8], and a textbook from *Gurtin* [40] can be referenced for a more elaborate discussion.

For a simple shear case (Fig. 4(a and b)), let us assume that κ is the amount of shear and γ is the shear angle. Thus, shear strain $\kappa = \tan(\gamma)$. Let **y** represent the deformed configuration of the brain white matter RVE, which is initially positioned at **X**. Thus, the simple shear equation can be written as:

$$\boldsymbol{y} = (\boldsymbol{X_1} + \boldsymbol{\kappa X_2})\mathbf{e_1} + \boldsymbol{X_2}\mathbf{e_2} + \boldsymbol{X_3}\mathbf{e_3} \tag{4}$$

In **Equation (4)**, $\{\mathbf{e_1}, \mathbf{e_2}, \mathbf{e_3}\}$ denote the rectangular cartesian coordinate system basis vectors. This equation signifies the shear displacement boundary condition while inhibiting displacement in the normal direction. The resultant deformation gradient tensor, **F**, can be computed as (**Equation (5)**):

$$F = \frac{\partial \mathbf{y}}{\partial \mathbf{X}} = \begin{bmatrix} 1 & \kappa & 0 \\ 0 & 1 & 0 \\ 0 & 0 & 1 \end{bmatrix} \tag{5}$$

For soft tissues undergoing very large strains, nonlinear elastic models (such as hyperelastic (HE) constitutive models) adequately describe the resultant deformation mechanism. For HE materials, the Cauchy stress tensor (**Equation (11)**) is derived as discussed in **§2.2**

$$C = F^T F = \begin{bmatrix} 1 & \kappa & 0 \\ \kappa & 1+\kappa^2 & 0 \\ 0 & 0 & 1 \end{bmatrix} \tag{6}$$

In general, Ogden hyper-elastically modeled soft tissues' strain energy density function W is a function of two principal invariants only $W = W(I_1, I_2)$, where $I_1 = tr(C)$, $I_2 = \frac{1}{2}({I_1}^2 - tr(C^2))$. But for simple shear case, $I_1 = I_2 = 3 + \kappa^2$. C is derived as shown in **Equation (6)**. The shear component of the Cauchy stress tensor is described as (**Equation (7)** [41]):

$$\sigma_{12} = 2\kappa \left(\frac{\partial W}{\partial I_1} + \frac{\partial W}{\partial I_2}\right) \tag{7}$$

Thus, $W = W(3+\kappa^2, 3+\kappa^2) \equiv \widehat{W}(\kappa)$ refer to Rashid et al. [8] for more details on the constitutive derivations. Soft tissues are often characterized well by Ogden model formulation, and a lot of mechanical test data for brain white matter tissues fits the Ogden hyperplastic (HE) function, hence backing its selection as a constitutive model for this research. The one-term Ogden HE functions is given by (**Equation (8)**):

$$W = \frac{2\mu}{\alpha^2}\left(\lambda_1^{\alpha} + \lambda_2^{\alpha} + \lambda_3^{\alpha} - 3\right) \tag{8}$$

In **Equation (8)**, λ_i are the principal stretch ratios (the square roots of the eigenvalues of C). In simple shear models, the principal stretch ratios can be computed as follows:

$$\lambda_1 = \frac{\kappa}{2} + \sqrt{1 + \frac{\kappa^2}{4}}, \lambda_2 = {\lambda_1}^{-1} = -\frac{\kappa}{2} + \sqrt{1 + \frac{\kappa^2}{4}}, \lambda_3 = 1 \tag{9}$$

Using **Equation (9)** in **Equation (8)**, we get the resultant expressions for W and σ_{12} as depicted in **Equation (10)** and **Equation**

Table 1
HE material properties summary of single-RVE FEM [28,37].

Material Component	μ MPa	D 1/MPa	α	Element Type
Axon	2.15E-03	0	6.19	C3D8RH
ECM	8.5 E−04	0	6.19	C3D8RH

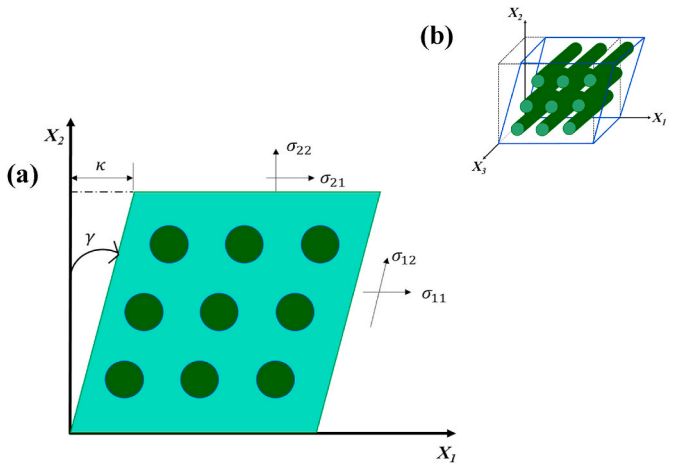

Fig. 4. (a) Schematic diagram analytically representing simple shear; the shear strain is denoted as κ along X_1 direction. (b) Simple shear deformation. Here, dotted lines: represent sample in the undeformed configuration; solid lines: deformed sample [7].

(12).

$$\widehat{W}(\kappa)=\frac{2\mu}{\alpha^2}\left[\left(\frac{\kappa}{2}+\sqrt{1+\frac{\kappa^2}{4}}\right)^{\alpha}+\left(-\frac{\kappa}{2}+\sqrt{1+\frac{\kappa^2}{4}}\right)^{\alpha}-2\right] \tag{10}$$

In the generalized Cauchy Stress tensor formula for isotropic homogenous hyperelastic materials of the Ogden form (see Equation (11)), the normal and shear stress components can be represented as shown in Equations (12)–(14). In Equation (11), p represents the Lagrange multiplier introduced by the constraint of incompressibility (described in **§2.2**).

$$\sigma_{ij}=-p\delta_{ij}+\lambda_i\frac{\partial W}{\partial\lambda_j} \tag{11}$$

As noted in Equation (11), the Cauchy stress tensor is typically comprised of normal and shear components with respect to the defined coordinate system. The normal stress component (σ_{ij}) in the j-th principal direction is associated (i.e., $i=j$, σ_{jj}: normal stress terms) with the hydrostatic pressure term ($-p\delta_{ij}$). The hydrostatic pressure acts equally in all directions and is responsible for the normal stress term. The second term of Equation (11) signifies the shear stress acting on a plane with the normal in the i-th direction and tangent in the j-th direction (i.e., σ_{ij}: shear stress terms). Mathematically, shear stress components can be expressed as $\tau_{ij}=\sigma_{ij}$.

The σ_{22} term in Equation (14) is non-zero. The presence of this non-zero normal stress (σ_{22}), and the inequality $\sigma_{11}\neq\sigma_{22}$ is an exhibition of the Poynting effect and is an outcome of material non-linearities in hyperelastically modeled brain white matter soft tissues [39].

$$\sigma_{12}=\widehat{W}'(\kappa)=\frac{\mu}{\alpha}\frac{1}{\sqrt{1+\left(\frac{\kappa^2}{4}\right)}}\left[\left(\frac{\kappa}{2}+\sqrt{1+\frac{\kappa^2}{4}}\right)^{\alpha}-\left(-\frac{\kappa}{2}+\sqrt{1+\frac{\kappa^2}{4}}\right)^{\alpha}\right] \tag{12}$$

$$\sigma_{11}=\frac{2\mu}{\alpha}\left[\left(\frac{\kappa}{2}+\sqrt{1+\frac{\kappa^2}{4}}\right)^{\alpha}-1\right] \tag{13}$$

$$\sigma_{22}=T_{22}=\frac{2\mu}{\alpha}\left[\left(\frac{\kappa}{2}+\sqrt{1+\frac{\kappa^2}{4}}\right)^{-\alpha}-1\right] \tag{14}$$

In their study on the one-term isotropic Ogden model for soft tissues [29], Horgan and Murphy share insights on nonlinear elastic materials and the gap between current analytical models and actual physical realization by considering three boundary condition scenarios. They point out that extra Ogden invariants could help attain a more rational and reliable prediction of the Poynting effect for complex geometries and boundary conditions. In their analytical model, they derive an expression for traction (T) and shear forces (S) That arises on the inclined faces to maintain the state of simple shear. Their analysis revealed that a theoretical optimal value of $\alpha=6$ (in Equation (8)) could negate the need to impose any normal traction forces (N) on the inclined faces to analytically realize simple shear for one-term Ogden hyperelastic soft tissues. Such a configuration would manifest a moderate tensile hydrostatic stress (H) and moderate positive normal stress (T_{22}) (same as σ_{22} in this paper) for moderate amounts of shear, it also proved the computational feasibility of the shear strain limits explored in the POC FEM model described in later sections.

$$T_{33} = \sigma_{33} = \frac{2\mu}{\alpha}\left(\frac{(\lambda^{\alpha}-1)(\lambda^{6-\alpha}-1)}{1+\lambda^{6}}\right) \tag{15}$$

$$H = \frac{2\mu}{\alpha}\left(1+\frac{\lambda^{\alpha+6}-2\lambda^{\alpha}+\lambda^{-\alpha}-2\lambda^{6-\alpha}}{1+\lambda^{6}}\right) \tag{16}$$

Following the case of zero normal traction on the inclined faces from Horgan's research [42,43], out-of-plane stress (T_{22}). For the Ogden modeled HE brain soft tissues, resultant out-of-plane stress (T_{33}) and the hydrostatic stress (H) are obtained as depicted in **Equation (15)** and **Equation (16)** (Note: notations T_{33} signify σ_{33} in this paper). For convenience, let us set $\lambda_1 \equiv \lambda$ and $\lambda_2 = 1/\lambda_1$. While exact congruence between analytical models and computational results is difficult, the proposed Ogden model for simulating Poynting effect can perform reasonably well to yield reasonable stress profiles.

One should note that, a computational framework perspective, in numerical tools such as Abaqus (General, explicit) solver, these constitutive equations should not be misinterpreted as homogenized representations for entire RVEs. Instead, the constitutive Equations (4)–(16) are computed for both axon and ECM phase elements (using corresponding material parameters – Table 1). Then, the FE solver returns the max. Nodal computed values representing output parameters such as the normal stress, displacement, and von Mises stress. These are then plotted in subsequent sections to describe the resultant Poynting effect. Thus, to eliminate redundancies, all constitutive equations are described without any material phase subscripts (W_{axon} *or* W_{ECM}). However, it is implied that the solver numerically performs these computations for axons and ECM mesh elements. Hence, analytical model equations are discussed for simplicity without material phase subscripts.

2.4. Finite element model

In the current study, as a POC for realizing the Poynting effect in brain white matter, a micromechanical scale Representative volume element (RVE) geometry of unit dimensions (1 μm × 1 μm x 1 μm), packing two axons in ECM material is designed to set up a finite element method (FEM) model to depict Poynting effect in various simple shear configurations. In the proposed FEM, axons are tied to the surrounding ECM.

Axon fibers are modeled as straight cylindrical fibers with an average diameter of 0.44 μm. Proposed RVEs have two effective axons packed with a volume fraction of VF = 0.3 to analyze for Poynting behavior. Refer to Fig. 5(a–d) for FEM geometrical setup details. The FEM used a mesh of 81,520 elements. Hybrid hexahedral elements (C3D8RH: An 8-node linear brick, hybrid, constant pressure, reduced integration, hourglass control). All elements required a linear hybrid formulation due to the hyperelastic material assignment to reproduce exact incompressibility. To model the axon and ECM material phases, the Ogden HE material model was deployed as discussed in **§2.2** and **§2.3** to account for hyper-elasticity.

FE Model Boundary Conditions: To simulate a simple shear scenario, one face is fixed (encastered) to depict the face of a tissue sample fixed on a platform. The surface to be sheared in a given direction is pinned in the other two directions to maintain a state of simple shear. A strain value is specified for the corresponding shear model in the ensemble of cases discussed here. A reference point

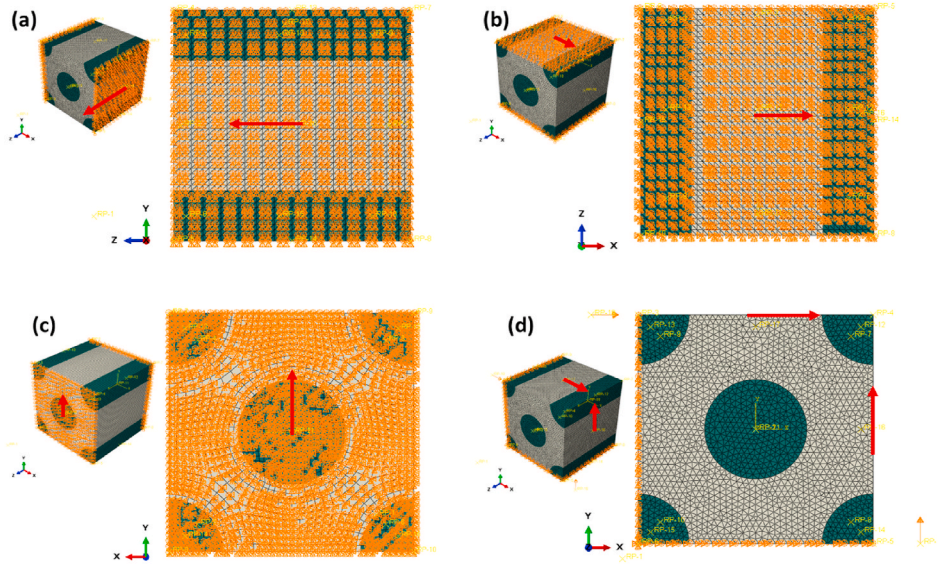

Fig. 5. (a) FEM describing simple shear along axon fiber (longitudinal shear) for a single RVE FEM, with the back face fixed and a shear stretch applied on the front face. (b) FEM for the simple shear across axonal fibers. (c) FEM setup for simple shear perpendicular to fiber (along the y-axis). (d) Pure shear FEM B.C. setup with shear applied across the axon axis on two RVE faces.

(RP) was defined at the center of the face. The surface subjected to simple shear has the RP that is kinematically coupled to all the points on the edge nodes of the RVE face. The linear shear strain value is defined and solved to 100% shear strain. The field output values of particular interest are stress (S) and displacement (U) field variables.

3. Results and discussion

In this paper, the developed micromechanical FEM is subjected to three simple shear scenarios. These cases are: 1. Simple shear along the axon (shear along z-direction), 2. Simple shear across the axon fiber tracks (i.e., shear along X-direction) and 3. Simple shear perpendicular to the axon fibers (i.e., shear along Y-direction). A fourth case of pure shear is also experimented with to investigate the extent of Poynting behavior. As a representative case, the FEM contour plot for single-RVE shear along axon fiber and ECM material combination is shown for the Static, General FE simulation step case. The shear moduli for axon and ECM are derived from Table 1, as discussed in §2. Fig. 7(a–d) shows the pure shear FEM contour plots for stress distribution for 20% shear strain applied. The difference in stiffness between axon and ECM phases and the inherent nonlinear hyperelastic material characteristics lead to the manifestation of Poynting behavior.

Comparing normal stress and deformation profiles revealed that Poynting behavior was predominant for simple shear cases along axon fibers at lower strain limits. At 20% strain, the pure shear RVE model yielded normal shear at 36.2% and 19.6% of Von-mises (S) and total deformation (U), indicating some Poynting behavior. The difference in the shear moduli of the axon and ECM phases contributed to the degree of deformation, leading to the Poynting effect in the bi-phasic model (see Fig. 6(a–d)).

3.1. Simple shear along fiber – RVE FEM model

For simple shear along the axon fiber axis (Case I) RVE configuration, Fig. 8 shows the stress vs. strain profiles. This model is based on the boundary conditions described in §2.4 (see Fig. 5(a)). Simple shear is applied on the *XZ surface*. The stress is normal to the direction of shearing (S11) and is monitored to describe Poynting behavior. At 100% strain (i.e., 45 deg simple shear strain) [44], the maximum value of the positive normal stress S11 is 34.5% of the max. Von-mises stress (S) and max. directional deformation normal to the shear direction (U1) is 10.5% of the max. total deformation (U), indicating modest (see Fig. 9) Poynting behavior when sheared longitudinally along the axon fiber axis (along the z-axis). In each of the analyzed RVE cases, RMSD analysis is conducted to calculate the variation in stress profile, von Mises vs. normal stress component, perpendicular to shear planes in all four shear RVE models. Root-Mean-Square Deviation (RMSD) is defined as: $\sqrt{\sum \frac{(f(x_i)-g(x_i))^2}{N}}$ for curves $f(x)$, $g(x)$ and N being number of points x_i at which curves

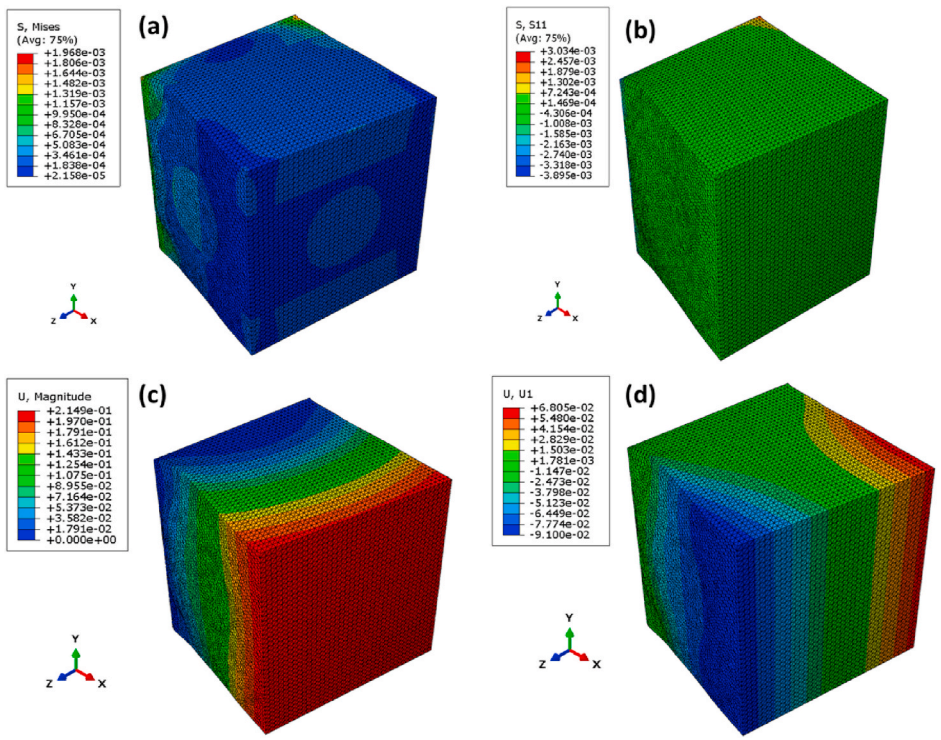

Fig. 6. (a) Von Mises stress contour (S) for the axons and the ECM at 20 percent applied stretch for single RVE FEM (shear along axon fiber axis – longitudinal shear). (b) The normal stress (S11) component is perpendicular to the direction of applied shear (along the z-axis). (c) Total deformation (U) plot at 20% applied shear strain. (d) U1 is normal to the applied shear strain plane, depicting positive Poynting behavior.

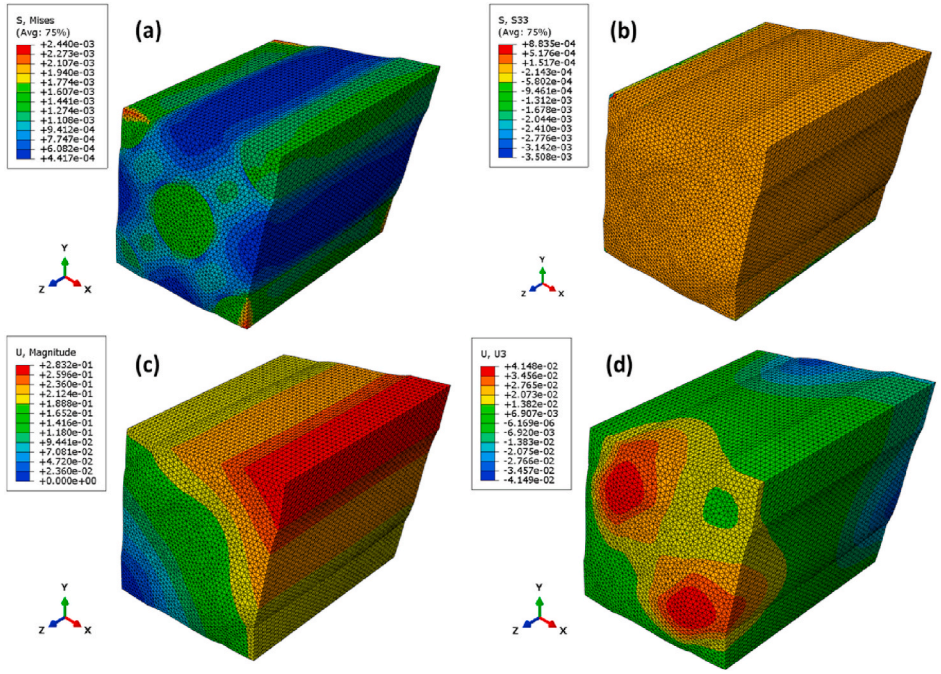

Fig. 7. (a) Von Mises stress (S) for axons and ECM at 20 percent applied stretch for single RVE FEM (pure shear). (b) The normal stress (S33) component is perpendicular to the direction of applied shear on the pair of opposite faces across axon fibers. (c) Total deformation (U) plot at 20% applied pure shear strain. (d) U3 is normal to applied pure shear strain planes, depicting the modest positive Poynting effect.

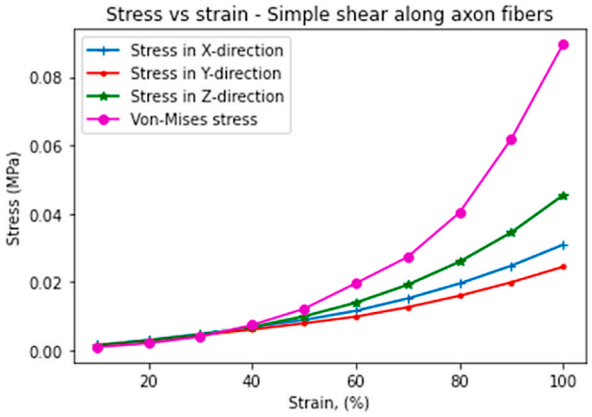

Fig. 8. Stress (σ) versus strain (ε) % plot single-RVE FEM for simple longitudinal shear (along *z-dir.)* depicting the impact of axonal direction on the resultant Poynting Effect (PE) (Case I). RMSD between S (*von-Misses*) and S11 (*x-dir.*) is 0.03022 and between S11 and S22 (*y-dir.*) is 0.00384.

are compared. RMSD between von-Mises (S) and normal stress (S11) for Case 1 (*simple shear along axon fibers, x-dir.*) is found to be 0.03022. Meanwhile, RMSD between S11 and S22 (*y-dir.*) curves (Fig. 8) are calculated as 0.00384, showing that in both transverse directions to shear planes, the normal stress profiles are similar in magnitude.

RMSD analysis between the deformation plots U3 (shear direction) and U1 (direction normal to shear) is 0.7535. Similarly, RMSD between U1 and U2 were calculated to be 0.0355, indicating that a similar degree of normal deformation was observed in both transverse directions to shear planes. With increasing simple shear strains, the normal deformation component remained fairly constant (as shown in Fig. 9), denoting mild Poynting behavior in longitudinal shear configuration.

3.2. *Simple shear across fiber – RVE HE model*

As in case II, simple shear is applied to the single-RVE FEM across the fiber axis (i.e., the simple shear strain applied along the x-direction on the *XY surface*), Fig. 10 shows the stress vs. strain profiles. The boundary conditions are described in §2.4 (see Fig. 5(b)).

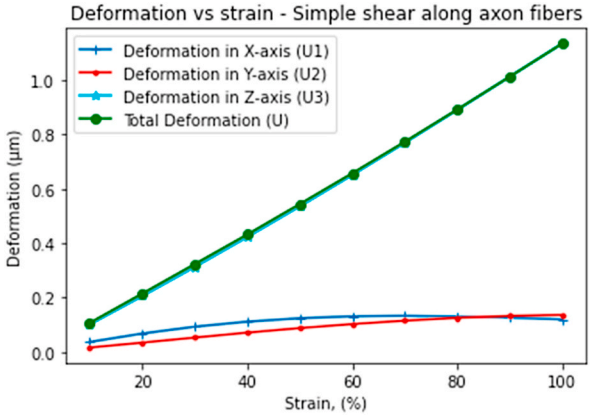

Fig. 9. Deformation (U, U1, U2, U3) versus shear strain (ε) % plot single-RVE FEM for simple longitudinal shear (along *z-dir.)* depicting impact of axonal direction on the resultant (PE) (Case I). RMSD between U3 (shear direction, z-dir.) and U1 (along *x-dir.*) is 0.7535 and between U1 and U2 (*y-dir.*) is 0.0355.

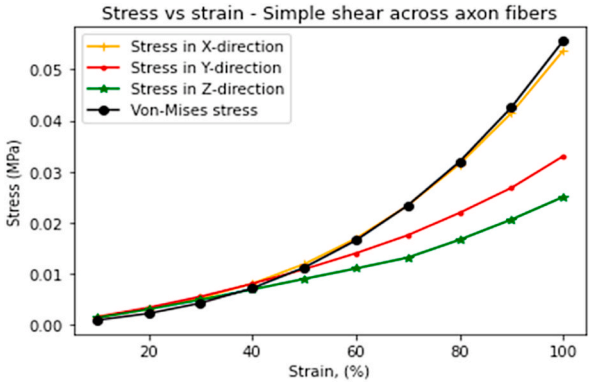

Fig. 10. Stress (σ) versus strain (ε) % plot single-RVE FEM for simple transverse shear (Case II), across axon fibers (along *x-dir.)*. RMSD analysis showed a more even distribution between normal stress profiles vs. von Mises stress and greater PE behavior compared to Case I. RMSD between S (*von-Misses*) and S22 (*y-dir.*) is 0.01227 and between S22 and S33 (*z-dir.*) is 0.00522.

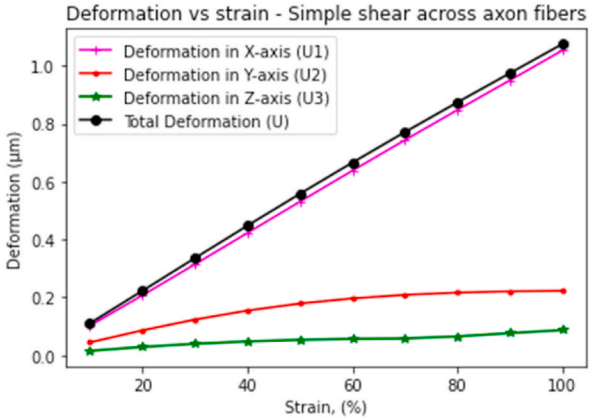

Fig. 11. Deformation (U, U1, U2, U3) versus shear strain (ε) % plot single-RVE FEM for transverse simple shear (along x-*dir.*) depicting impact of axonal direction on the resultant (PE) (Case II). RMSD between U1 (shear direction, x-dir.) and U2 (along *y-dir.*) is 0.6264 and between U3 and U2 (*y-dir.*) is 0.1543.

The S22 stress component is normal to the direction of shearing and indicates the extent of PE. At 100% strain, max. S22 is 59.6% of the max. Von-mises stress (S) and max. Positive directional deformation (U2), which is normal to the direction of simple shear (along the x-axis), is 20.6%, verifying the presence of Poynting behavior (Fig. 11). The second simple shear configuration described greater Poynting behavior than Case 1 (§3.1). This may be attributed to the fact that fibers in this simple shear are also subjected to some degree of stretching in the transverse direction, and hence, a greater magnitude of normal stress would be necessary to retain the state of simple shear experimentally. This is in line with the findings of *Destrade et al.* [22], who posited that soft tissues could have a dominant directional Poynting behavior.

RMSD between von Mises (S) and normal stress (S22) for Case II is found to be 0.01227. This is less than the RMSD obtained in Case I, demonstrating comparatively greater Poynting behavior. Meanwhile, RMSD between S22 and S33 curves (Fig. 10) are calculated as 0.00522, implying that normal stresses in the transverse direction to shear planes are similar in magnitude.

RMSD between deformation plots U1 (shear direction) and U2 (direction normal to shear) are 0.6264 (Fig. 11). The decreasing RMSD value clearly describes the greater relative positive Poynting effect (*compared to Case I*). RMSD between U3 and U2, calculated to be 0.1543, verified that transverse shear led to a dominant stretching across axonal fibers (along the y-axis) and, hence, more obvious positive directional deformation (PE).

3.3. Simple shear perpendicular to fiber – HE model

For the final simple shear model (Case III), simple shear is applied to the single-RVE FEM perpendicular to the fiber axis (i.e., the simple shear strain applied along the y-direction on the *YZ surface*), Fig. 12 plots the stress vs. strain trends. In this FEM, as per the boundary conditions defined in §2.4 (see Fig. 5(c)). The S33 stress component is normal to the direction of shearing and indicates the extent of Poynting behavior. At 100% strain, max. S33 is calculated to be 43.95% of the max and observed von Mises Stress (S). A more evenly distributed stress profile is observed along all axes in this configuration. The S22 curve (red curve in Fig. 12) also proved the existence of directional stretch in axonal fibers when sheared perpendicularly to the fiber axes. This corroborates with the theoretical models put forward by Destrade et al. [22], which underscores the directional dependence of the Poynting effect in sheared brain white tissues.

RMSD between von Mises (S) and normal stress (S33) for Case III is found to be 0.01206. It is less than the RMSDs obtained in Case I & II (stress profiles), demonstrating the greatest Poynting behavior amongst three simple shear models. It was also validated by comparing max. Normal stress values were 8.64% higher in Case III than in Case II. RMSD between S11 and S33 curves (Fig. 12) is calculated as 0.00673, verifying that the y-axis is the prominent transverse direction exhibiting the Poynting effect [21,39].

RMSD between deformation plots U2 (shear direction) and U3 (direction normal to shear) is 0.7556. There is a slightly higher RMSD value between deformation curves than in Case II. The positive Poynting effect is still exhibited in Cases I & *and II*. Deformation analysis (Fig. 13) revealed that the normal deformation component (U3) is 9.55% of the max. deformation (along the y-axis) in Case III. Thus, describing a modest Poynting effect. Although, RMSD between U1 and U3 were determined to be 0.05323, suggesting that contribution from higher order invariants by incorporating other material models (such as transverse isotropic or anisotropic hyperelastic) can be explored to determine more perceptible positive Poynting behavior in Case III configuration [22]. Such models would require traction forces to be applied on the side faces to maintain simple shear; hence, more pronounced directional positive or negative deformation depicting Poynting behavior could come to light [17]. Nevertheless, the proposed P.O.C. FEM stress profiles confirm Poynting behavior in Case III.

3.4. Pure shear model – HE model

While many research studies have delved into the Poynting effect for the twisting of cylindrical white matter tissues, few numerical

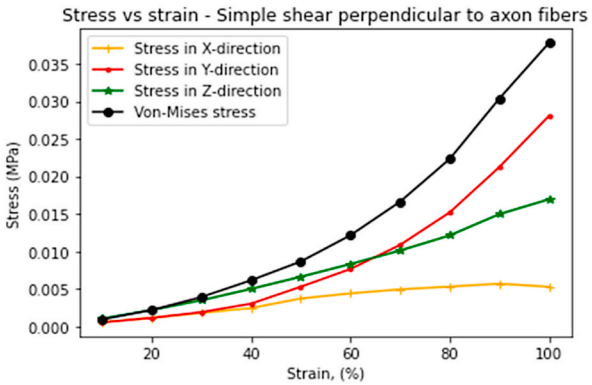

Fig. 12. Stress (σ) versus strain (ε) % plot single-RVE FEM for simple perpendicular shear (Case III), normal to axon fibers axes (along *y-dir.)*. Axonal fiber stretching contributed to significantly higher normal stresses. Perpendicular stresses (S33, along *z-dir.*) normal to the shear plane (green curve) also suggest greater PE behavior than Case I. RMSD between S (*von-Misses*) and S33 (*z-dir.*) is 0.01206 and between S11 and S33 (*z-dir.*) is 0.00673.

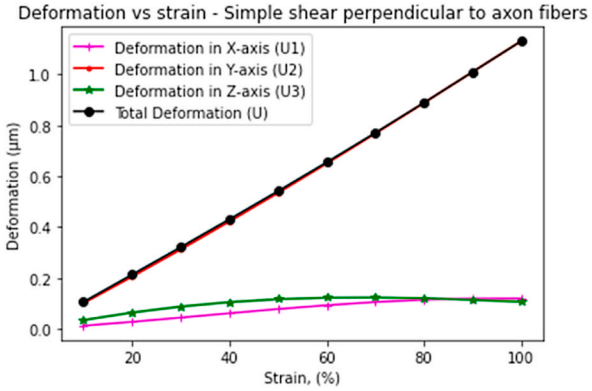

Fig. 13. Deformation (U, U1, U2, U3) versus shear strain (ε) % plot single-RVE FEM for perpendicular simple shear (along y-*dir.*) depicting impact of axonal direction on the resultant (PE) (Case III). RMSD analysis was done on the deformation results (U3) vs U to quantify variations in resultant PE behavior with increasing shear strain RMSD between U2 (shear direction, y-dir.) and U3 (along *z-dir.*) is 0.7556 and between U1 and U3 (*z-dir.*) is 0.05323.

models have explored the numerical realization of pure-sheared rectangular brain matter specimens for the Poynting effect. In this regard, a fourth case was analyzed to model single-RVE subjected to pure shear boundary conditions (B.C.). In this FEM setup, shear strains are applied along x- and y-directions on the *YZ and XZ surfaces*) respectively. Fig. 5(d) depicts the FEM B.C. for pure shear RVE analysis. Fig. 14 plots the stress vs. strain trends. For the pure shear model, at strains close to 60%, the stress profiles increase dramatically, and this could be attributed to stress concentrations on the stretched axonal fibers when subjected to pure shears. This exponential rise can also be due to numerical factors whereby the maximum von-mises for axonal node elements act as stress concentration zones due to some degree of bending that occurs in the fibers.

When analyzed for strains beyond 60%, the single-RVE pure shear FEM model suffered convergence issues due to excessive distortions in the hybridized FEM elements. However, as past analytical models from literature and experimental studies hypothesized, solving for strain up to 60% did imply that the proposed model with linearized hybrid elements could computationally depict previously attained extension limits [8] on brain tissues to describe the Poynting effect. In the future, the present single-term Ogden model can be expanded to include the high-order invariants, and computationally high-order (quadratic hybrid FEM elements) may be explored to check model efficacies for extreme pure shear strain limits.

From Fig. 14, the max. stress analysis revealed that the normal stress component (S33) to planes of pure shear was 13% of the max. recorded von Mises stress. The high RMSD between the von Mises and normal stress curves is due to the high shear stress terms contributing to the overall von Mises magnitude. Tensile directional deformation (U3) revealed 26% of the total deformation (U) (Fig. 15) and confirmed the presence of positive Poynting behavior in pure shear RVEs. RMSD between von Mises (S) and normal stress (S33) for Case IV (*pure shear model*) is found to be 0.15631 (Refer Fig. 14). It is the highest RMSDs obtained for stress profiles, which could be mainly due to computational reasons on excessively distorted hybrid pure-sheared elements. RMSD between S11 and S33 were observed to be 0.03394, underscoring that when subjected to pure shear fiber, it also experiences stretching, and there is still a consequent normal stress (S33) normal to pure shear planes describing net positive Poynting behavior.

RMSD between total deformation (U) and U3 curves (refer Fig. 15) are calculated as 0.42967, the least RMSD among all four analyzed configurations, indicating the greatest relative Poynting behavior at higher strains up to 60% due to stress concentrations arising in bending axons subjected to pure shear. It is also supported by a lower RMSD value (0.26345) between pure shear and normal deformation (U3), verifying enhanced resistance to shear in pure shear conditions.

3.5. Comparison of Poynting behavior (all cases)

Manifestation of the Poynting effect in nonlinear materials depends on geometrical factors and material parameters and is also highly influenced by the nature of the shear or twist applied [14]. Hence, a comparative numerical analysis is merited to understanding how the Poynting effect varies with different shear load cases when analyzed using a single-RVE FEM setup. This section compares all four previously discussed cases to quantitatively describe variation in the Poynting effect in the bi-phasic brain white matter FE model. For this, the RMSD analyses are performed to determine variations in Poynting behavior in terms of normal stress and normal deformation components.

The Poynting behavior in nonlinear models is often characterized or modeled by two major parameters. One of the metrics is the presence of stresses normal to the direction of applied shear; another is positive or negative deformation normal to the shear direction. RMSD analysis for the stress profiles for all four analyzed cases yielded that in terms of stress, Poynting behavior increased as follows: Case II < Case III < Case I < Case IV (pure shear) FEM model. RMSD between Case I and Case III, 0.00184 < Case I and Case III, 0.00297< Case I and Case IV, 0.01887 (refer Fig. 16). Hence, all simple shear models show a similar degree of Poynting behavior. However, excessive bending and shear distortions build-up in the pure shear model meant that Case IV requires a much higher amplitude of normal stress component to maintain a state of pure shear in brain white matter, i.e., indicating the greatest degree of

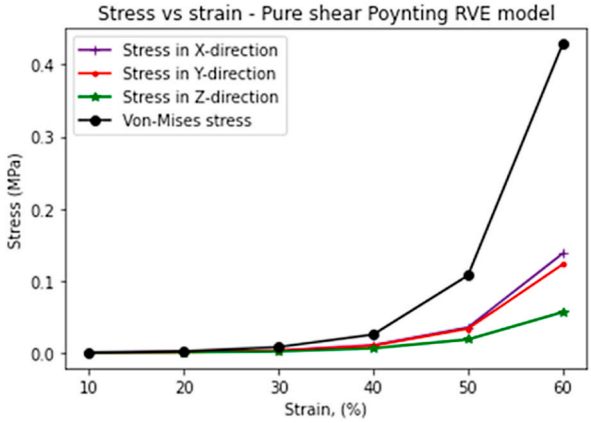

Fig. 14. Stress (σ) versus strain (ε) % plot single-RVE FEM for pure shear (strain on pair of faces across fibers - Case IV). Some degree of axonal bending contributed to an exponential rise in normal stresses. Perpendicular stresses (S33) normal to shear planes proved the existence of positive Poynting behavior in pure-sheared brain matter. RMSD between S (*von-Misses*) and S33 (*z-dir.*) is 0.15631 and between S11 and S33 (*z-dir.*) is 0.0339, underscoring that when subjected to pure shear fiber, it also experiences stretching, and there is still a consequent normal stress (S33) normal to pure shear planes describing net positive Poynting behavior.

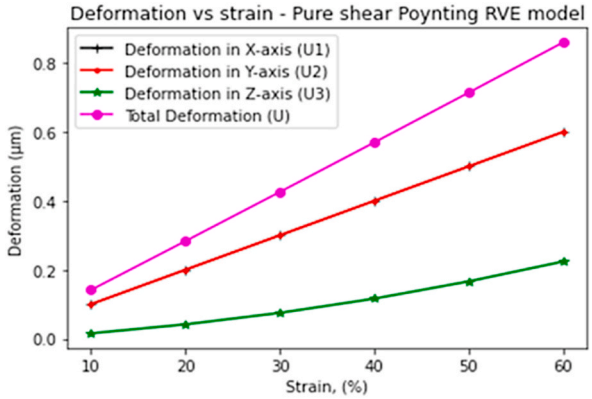

Fig. 15. Deformation (U, U1, U2, U3) versus shear strain (ε) % plot single-RVE FEM for pure shear strained (Case IV). RMSD analysis was done on the deformation results (U3) vs. U to quantify variations in resultant PE behavior with increasing shear strain. RMSD between U and U3 is 0.42967 and between pure shear and U3 (*z-dir.*) is 0.26345.

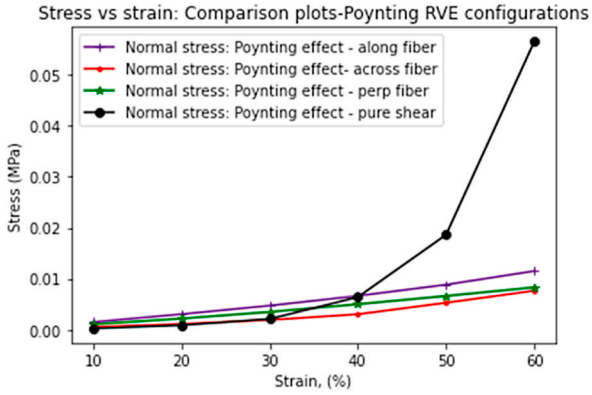

Fig. 16. Stress (σ) versus shear strain (ε) % plots of single-RVE FEM comparing the extent of demonstrated PE in all four configurations (Case I -IV). Excessive distortions led to high stress concentration in the pure shear model (black curve). All four models verified the existence of positive Poynting behavior.

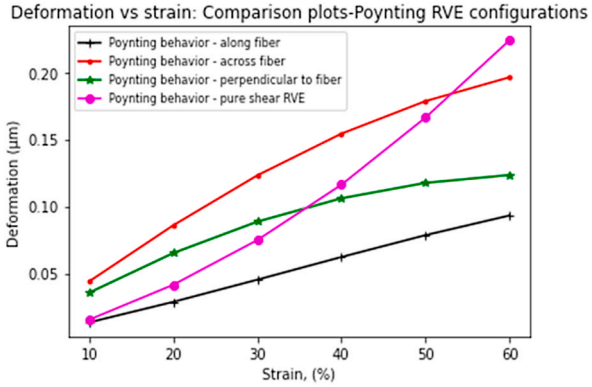

Fig. 17. Deformation (U, U1, U2, U3) versus shear strain (ε) % plots for all four single-RVE FEM (Case I-IV). RMSD analysis revealed a transitional trend in the extent of positive Poynting behavior, with a pure shear model due to bending stresses in axons at higher strains.

Poynting effect among all analyzed models.

RMSD analysis for the deformation plots showed a transitional behavior in the degree of the Poynting effect. In Fig. 17, RMSD between Case I (black curve) and Case III (green curve) is 0.0054 < RMSD between Case I and Case II (red), 0.0412 < RMSD between Case I and Case IV/pure shear model (pink), 0. 04437. It is clear to see that at lower strain limits, simple shear applied across fiber and perpendicular to axonal fibers showed a dominant Poynting effect, but as the strains were increased to 60%, excessive shear deformations in pure shear RVE model led to a pronounced positive Poynting displacements along the z-axis (U3, as discussed in **§3.4**).

3.6. FE model verification and validation

As discussed in **§1.3** and **§1.4**, the proposed micro-mechanical 3D FEM corroborated with several key findings from previous research, such as the role of axonal fiber-matrix interactions on the resultant Poynting effect [21]. While many researchers simulated shear tests at varying strain rates, the non-linear resultant Poynting behavior is also evident for quasi-statically modeled hyper-elastic (**HE**-defined) brain white matter. Dominant Poynting effect in certain loading scenarios was also observed in the proposed bi-phasic 3D FEM, as illustrated in **§3.5.** The resultant stress and displacement plots also showed similar qualitative trends by consistently manifesting positive Poynting behavior [23] in all four evaluated shear configurations, as discussed in **§3**. Similarly, comparing the normal stress trends with results from *Rashid et al.* [8], it is observed that Ogden-modeled brain matter in the current study corroborates with the non-linear trend seen in their one-term Ogden non-linear shear model subjected to simple shear at varying strain rates. However, such validation is qualitative only since their model was at a different scale (mm) and defined with their own obtained material properties. Nevertheless, similarity in non-linear trends strongly suggests scalability in non-linear stress build-up in brain white matter. Accurate experimental characterization of brain white matter at micro-scale is extremely difficult and mechanical test at axonal tract level is not feasible due to technological limitations. Hence, one-on-one experimental validation of proposed POC micro-mechanical Poynting 3D FEM is not feasible due to challenges in extracting brain matter properties at the micro-scale when singular axons are subjected to shear. The qualitative congruency in **§3** for respective shear ensemble cases and key research outcomes discussed in **§1.3** provide sufficient qualitative evidence and promise in directional dominance and confirm the effects of RVE geometric factors on resultant Poynting effect in brain white matter.

4. Conclusion

Shearing of nonlinear tissues is not a simple phenomenon; it is often accompanied by normal forces resulting from material nonlinearities. This coupling of normal and shear tractions for brain white matter (axon and glial tissues) leads to the Poynting effect. From a physiological and biomedical standpoint, numerical modeling of the PE in nonlinearly behaving soft tissues has found application in surgical planning and tissue-surgical tool interaction simulations [39].

A series of simulations are carried out for three simple shear FE models, and a fourth pure-shear model is analyzed to depict the Poynting effect using a Steady state (general, static) setup in Abaqus. For simple shear models, Ogden HE modeled brain white matter showed evidence of the Poynting effect in all analyzed configurations. A positive Poynting effect (tissue expanding in the direction normal to shear direction) was observed for single-RVE FEM. At lower strains, longitudinally sheared axons (Case I) showed greater Poynting behavior, but as strain limits were gradually increased, shear deformation build-up in the pure shear model (Case IV) exhibited the highest directional deformation normal to shear planes. FEM results also proved that loading configuration does affect the degree of Poynting effect as in Case II and Case III, axonal fibers undergo some degree of stretching and hence greater Positive Poynting behavior (Fig. 17). In all analyzed cases, numerical results suggested that specimen thickness was seen to have no influence on shear stresses for an isotropic Ogden HE-modeled brain white matter RVE. However, if more RVEs are joined, stresses are expected to scale up. This aligns with numerical studies conducted by *Rashid et al.* [8], who observed similar thickness independence for homogenized brain matter models subjected to shear loads.

The proposed proof-of-concept micromechanical FEM has potential limitations. First, the model approximates tie-contact between axon and ECM phases, although physiologically, they exhibit more transitional kinematics [26,32,36]. FE models with surface traction interactions defined between axon and ECM are being developed and could yield models with greater fidelity [21]. In this model, only one single-RVE FEM was presented as POC; in the future scalable RVE models will be examined to analyze shear stress build-up. In the future, more 3D RVE models with built-in axonal tortuosity will be developed to determine its effect on Poynting behavior. This model would help evaluate cerebral damage mechanics and its dependence on axonal geometry, varying brain mass, and shear loading magnitude.

Fiber packing will be parameterized in future test cases to understand stress build-up in densely packed RVEs. Also, the authors propose that aging in brain matter can be computationally characterized by tuning the volume fractions (VF) for myelinated axons to analyze the effect of shear loads on hyper-elastically defined decaying or injured brain matter [25,45]. This would enhance our understanding of stress relaxation and tissue softening behavior in an aging brain. It would also aid investigate how alterations in the brain's microstructure, mechanical properties, and overall shape, as modeled, impact the biomechanics of brain tissue. The authors posit that the proposed POC micromechanical models could translate processes at the microscopic scale into the evolution of mechanical properties and brain shape on the macroscopic scale. It would help facilitate the overarching goal of modeling the lifecycle of the brain and further refine existing modeling approaches to model brain injury, brain damage, and brain protection to shear or other load case scenarios [46]. While many previous studies have proposed mathematical or macroscopic (homogenized) computational modeling of Poynting behavior, this study is a novel attempt to help bridge the gap between macro-scale and microscale shear mechanics and pave the way for transitional multi-scale characterization of Poynting effect in scalable brain tissue FEM. Computationally feasible and elaborate 3D FEM explicit dynamics model with time-domain hyper-viscoelastic models could offer tremendous insights into damage initiation and bending stress in RVEs with tortuous axonal tracks. A recent study that used ultrasound shear waves elastography, showed that brain stiffness reduced with increasing temperature. It would be intriguing to explore such temperature effects by developing coupled field models to simulate brain tissue simple/pure shear states to determine variation in Poynting behavior with respect to temperature and surrounding conditions [47]. Two or three-term Ogden HE material models could be explored to simulate numerically the contributions of high-order invariants to validate dominant positive or negative Poynting behavior numerically [22] of different soft tissues.

Data availability statement

Data will be made available on request.

CRediT authorship contribution statement

Mohit Agarwal: Writing – review & editing, Writing – original draft, Validation, Formal analysis, Data curation, Conceptualization. **Assimina A. Pelegri:** Writing – review & editing, Validation, Supervision, Resources, Project administration, Investigation, Conceptualization.

Declaration of competing interest

The authors declare the following financial interests/personal relationships which may be considered as potential competing interests:Assimina A. Pelegri reports financial support was provided by National Science Foundation. Assimina A. Pelegri reports a relationship with Rutgers The State University of New Jersey that includes: employment.

Acknowledgements

NSF Grants CMMI-1436743, CMMI-1437113, CMMI-1762774, CMMI-1763005 provided support. The opinions, findings, conclusions, or recommendations expressed are those of the author(s) and do not necessarily reflect the views of the National Science Foundation.

Nomenclature

α	alpha
μ	shear moduli (hyper-elastic: Ogden model)
λ	principal stretches
σ	principal stress
τ	shear stress
W	Ogden strain-energy density function
F	Deformation gradient tensor
C	Cauchy-Green deformation tensor (right)
MRE	Magnetic Resonance Elastography
MRI	Magnetic Resonance Imaging

References

[1] G. Saccomandi, L. Vergori, Generalised Mooney–Rivlin models for brain tissue: a theoretical perspective, Int. J. Non Lin. Mech. 109 (2019) 9–14, 0020-7462.
[2] K. Miller, K. Chinzei, Mechanical properties of brain tissue in tension, J. Biomech. 35 (4) (2002) 483–490, 0021-9290.
[3] S. Budday, G. Sommer, C. Birkl, C. Langkammer, J. Haybaeck, J. Kohnert, M. Bauer, F. Paulsen, P. Steinmann, E. Kuhl, Mechanical characterization of human brain tissue, Acta Biomater. 48 (2017) 319–340, 1742-7061.
[4] S. Budday, G. Sommer, F. Paulsen, G. Holzapfel, P. Steinmann, E. Kuhl, Region-and loading-specific finite viscoelasticity of human brain tissue, Pamm 18 (1) (2018) e201800169, 1617-7061.
[5] X. Jin, F. Zhu, H. Mao, M. Shen, K.H. Yang, A comprehensive experimental study on material properties of human brain tissue, J. Biomech. 46 (16) (2013) 2795–2801, 0021-9290.
[6] S. Budday, G. Sommer, G. Holzapfel, P. Steinmann, E. Kuhl, Viscoelastic parameter identification of human brain tissue, J. Mech. Behav. Biomed. Mater. 74 (2017) 463–476, 1751-6161.
[7] M. Destrade, M.D. Gilchrist, J.G. Murphy, B. Rashid, G. Saccomandi, Extreme softness of brain matter in simple shear, Extreme Mech. Lett. 75 (2015) 54–58, 0020-7462.
[8] B. Rashid, M. Destrade, M.D. Gilchrist, Mechanical characterization of brain tissue in simple shear at dynamic strain rates, J. Mech. Behav. Biomed. Mater. 28 (2013) 71–85, 1751-6161.
[9] T.D. Wager, M.A. Lindquist, Principles of fMRI, Leanpub, New York, 2015.
[10] S. Budday, T.C. Ovaert, G.A. Holzapfel, P. Steinmann, E. Kuhl, Fifty shades of brain: a review on the mechanical testing and modeling of brain tissue, Arch. Comput. Methods Eng. 27 (2020) 1187–1230, 1134-3060.
[11] B. Donnelly, J. Medige, Shear Properties of Human Brain Tissue, 1997, pp. 148–731.
[12] M. Hrapko, J. Van Dommelen, G. Peters, J. Wismans, The mechanical behaviour of brain tissue: large strain response and constitutive modelling, Biorheology 43 (5) (2006) 623–636, 0006-355X.
[13] L. Shuck, S. Advani, Rheological response of human brain tissue in shear, 1972, 21-9223.
[14] V. Balbi, A. Trotta, M. Destrade, A.N. Annaidh, Poynting effect of brain matter in torsion, Soft Matter 15 (25) (2019) 5147–5153.
[15] R. Mangan, M. Destrade, G. Saccomandi, Strain energy function for isotropic non-linear elastic incompressible solids with linear finite strain response in shear and torsion, Extreme Mech. Lett. 9 (2016) 204–206, 2352-4316.
[16] P.A. Janmey, M.E. McCormick, S. Rammensee, J.L. Leight, P.C. Georges, F.C. MacKintosh, Negative normal stress in semiflexible biopolymer gels, Nat. Mater. 6 (1) (2007) 48–51, 1476-1122.
[17] L.A. Mihai, A. Goriely, Positive or negative Poynting effect? The role of adscititious inequalities in hyperelastic materials, Proc. Royal Soc. A: Math. Phys. Eng. Sci. 467 (2136) (2011) 3633–3646, 1364-5021.
[18] M. Askari-Sedeh, M. Baghani, Coupled chemo-mechanical swelling behavior of PH-sensitive hollow cylinder hydrogels under extension–torsion and internal pressure: analytical and 3D FEM solutions, Int. J. Appl. Mech. 15 (4) (2023) 1758–8251, 2350030.
[19] S. Niroumandi, M. Shojaeifard, M. Baghani, Finite deformation of swollen pH-sensitive hydrogel cylinder under extension and torsion and its Poynting effect: analytical solution and numerical verification, Int. J. Appl. Mech. 13 (6) (2021) 1758–8251, 2150071.
[20] A. Ghorbani, D. Dykstra, C. Coulais, D. Bonn, E. van der Linden, M. Habibi, Inverted and programmable Poynting effects in metamaterials, Adv. Sci. 8 (20) (2021) 2198–3844, 2102279.
[21] C. Horgan, J. Murphy, The effect of fiber-matrix interaction on the Poynting effect for torsion of fibrous soft biomaterials, J. Mech. Behav. Biomed. Mater. 118 (2021) 1751–6161, 104410.
[22] M. Destrade, C. Horgan, J. Murphy, Dominant negative Poynting effect in simple shearing of soft tissues, J. Eng. Math. 95 (2015) 87–98, 0022-0833.
[23] L.A. Mihai, A. Goriely, Numerical simulation of shear and the Poynting effects by the finite element method: an application of the generalised empirical inequalities in non-linear elasticity, Int. J. Non Lin. Mech. 49 (0020-7462) (2013) 1–14.
[24] M. Destrade, R.W. Ogden, Surface waves in a stretched and sheared incompressible elastic material, Int. J. Non Lin. Mech. 40 (2-3) (2005) 241–253, 0020-7462.
[25] M. Agarwal, P. Pasupathy, R. De Simone, A.A. Pelegri, Oligodendrocyte tethering effect on hyperelastic 3D response of injured axons in brain white matter, in: ASME International Mechanical Engineering Congress and Exposition vol. 85598, American Society of Mechanical Engineers, 2021. V005T005A050.
[26] M. Agarwal, A.A. Pelegri, Hyper-viscoelastic 3D response of axons subjected to repeated tensile loads in brain white matter, in: ASME 2022 International Mechanical Engineering Congress and Exposition. Volume 4: Biomedical and Biotechnology; Design, Systems, and Complexity, 2022. V004T05A046.
[27] C.O. Horgan, J.G. Murphy, The effect of fiber-matrix interaction on the kinking instability arising in the torsion of stretched fibrous biofilaments, J. Mech. Behav. Biomed. Mater. 124 (2021) 1751–6161, 104782.
[28] D.F. Meaney, Relationship between structural modeling and hyperelastic material behavior: application to CNS white matter, Biomech. Model. Mechanobiol. 1 (4) (2003) 279–293.
[29] Y. Pan, D. Sullivan, D.I. Shreiber, A.A. Pelegri, Finite element modeling of CNS white matter kinematics: use of a 3D RVE to determine material properties, Front. Bioeng. Biotechnol. 1 (2013) 2296–4185, 19.
[30] Y. Pan, D.I. Shreiber, A.A. Pelegri, A transition model for finite element simulation of kinematics of central nervous system white matter, IEEE Trans. Biomed. Eng. 58 (12) (2011) 3443–3446, 0018-9294.
[31] T. Brooks, J.E. Choi, M. Garnich, N. Hammer, J.N. Waddell, W. Duncan, M. Jermy, Finite element models and material data for analysis of infant head impacts, Heliyon 4 (12) (2018) e01010, 2405-8440.
[32] S. Singh, A.A. Pelegri, D.I. Shreiber, Characterization of the three-dimensional kinematic behavior of axons in central nervous system white matter, Biomech. Model. Mechanobiol. 14 (6) (2015) 1303–1315, 1617-7940.
[33] P. Pasupathy, R. De Simone, A.A. Pelegri, Numerical simulation of stress states in white matter via a continuum model of 3D axons tethered to glia, in: ASME 2020 International Mechanical Engineering Congress and Exposition, ASME, Portland, OR, USA, 2020. Volume 5: Biomedical and Biotechnology, V005T05A038.
[34] Abaqus, U.m.M., Standard, 2005, "Hibbitt, Karlsson, and Sorensen", 8,.
[35] M. Agarwal, P. Pasupathy, R. De Simone, A.A. Pelegri, Oligodendrocyte tethering effect on hyperelastic 3D response of injured axons in brain white matter, in: ASME 2021 International Mechanical Engineering Congress and Exposition, 2021. Volume 5: Biomedical and Biotechnology, V005T05A050.
[36] M. Agarwal, P. Pasupathy, A.A. Pelegri, Oligodendrocyte tethering effect on hyperelastic 3D response of axons in white matter, J. Mech. Behav. Biomed. Mater. 134 (2022) 1751–6161, 105394.
[37] X. Wu, J.G. Georgiadis, A.A. Pelegri, Brain white matter model of orthotropic viscoelastic properties in frequency domain, in: ASME International Mechanical Engineering Congress and Exposition vol. 59407, American Society of Mechanical Engineers, 2019. V003T004A024.
[38] K.B. Arbogast, S.S. Margulies, Material characterization of the brainstem from oscillatory shear tests, J. Biomech. 31 (9) (1998) 801–807, 0021-9290.
[39] S. Misra, K. Ramesh, A.M. Okamura, Modelling of non-linear elastic tissues for surgical simulation, Comput. Methods Biomech. Biomed. Eng. 13 (6) (2010) 811–818, 1025-5842.
[40] M.E. Gurtin, An Introduction to Continuum Mechanics, Academic Press, 1982.
[41] R.W. Ogden, Non-linear Elastic Deformations, Courier Corporation, 1997.
[42] C.O. Horgan, J.G. Murphy, Exponents of the one-term Ogden model: insights from simple shear, Philosoph. Trans. Royal Soc. A 380 (2234) (2022), 1364-503X, p. 20210328.
[43] C.O. Horgan, J.G. Murphy, On the normal stresses in simple shearing of fiber-reinforced nonlinearly elastic materials, J. Elasticity 104 (2011) 343–355, 0374-3535.
[44] M. Destrade, J.G. Murphy, G. Saccomandi, Simple shear is not so simple, Int. J. Non Lin. Mech. 47 (2) (2012) 210–214, 0020-7462.

[45] D.I. Shreiber, H. Hao, R.A. Elias, Probing the influence of myelin and glia on the tensile properties of the spinal cord, Biomech. Model. Mechanobiol. 8 (2009) 311–321, 1617-7959.
[46] S. Budday, E. Kuhl, Modeling the life cycle of the human brain, Curr. Opin. Biomed. Eng. 15 (2020) 16–25, 2468-4511.
[47] Y.-L. Liu, G.-Y. Li, P. He, Z.-Q. Mao, Y. Cao, Temperature-dependent elastic properties of brain tissues measured with the shear wave elastography method, J. Mech. Behav. Biomed. Mater. 65 (2017) 652–656, 1751-6161.